Water Practice & Technology

IWA PUBLISHING

Water Practice & Technology Vol 18 No 2, 295 doi: 10.2166/wpt.2023.005

Synthesis of cuprous oxide via ion exchange route for photocatalytic degradation of methylene blue

Xiangyao Liu [a,*], Haili Zhang[b] and Guolin Jing[b]

[a] School of Chemistry and Materials Science/Heilongjiang province, Heilongjiang University, Harbin 150080, China
[b] Chemistry and Chemical Engineering School/Heilongjiang province, Northeast Petroleum University, Daqing 163318, China
*Corresponding author. E-mail: liuxiangyao1@126.com

XL, 0000-0002-7576-1141

ABSTRACT

Cuprous oxide (Cu_2O) nanoparticles were successfully synthesized using cupric hydroxide gel as a precursor and glucose as a reductant. A well-dispersed cupric hydroxide gel was prepared by treatment of aqueous cuprous chloride with anion exchange resin. The average diameter of the Cu_2O nanoparticles was 780 nm. Attenuated total reflectance Fourier transform infrared spectroscopy showed that polyethylene from the anion exchange resin was present in the Cu_2O powder, explaining how the ion exchange route reduces agglomeration of the Cu_2O nanoparticles. Addition of hydrogen peroxide during the photocatalytic degradation of methylene blue significantly reduced photocorrosion of the Cu_2O nanoparticles. The mechanism by which hydrogen peroxide participates in the photocatalytic process and inhibits photocorrosion was investigated.

Key words: cuprous oxide, ion exchange resin, methylene blue, photocorrosion

HIGHLIGHTS

- Cuprous oxide nanoparticles were successfully synthesized via ion exchange route.
- Polyethylene in the ion exchange resin modifies the cuprous oxide nanoparticles and reduces agglomeration.
- The cuprous oxide was used for photocatalytic detoxification of methylene blue-contaminated water under visible light irradiation.

1. INTRODUCTION

Metal and metallic oxide nanoparticles have been extensively studied because of their extraordinary properties. Among metal oxide nanoparticles, cuprous oxide (Cu_2O), in particular, has received a great deal of attention in the field of photocatalysis. Cu_2O is a narrow gap, nontoxic, p-type semiconducting oxide that has been widely used in applications such as photocatalysis, self-cleaning pigments, antibacterial agents and solar cells because of its excellent photocatalytic activity under visible light. Cu_2O has been prepared by a variety of methods, including sonochemistry (Muthukumaran *et al.* 2020), liquid phase reduction (Yu *et al.* 2018), electro deposition (Sun *et al.* 2021), microwave irradiation (Kuo *et al.* 2014) and sol-gel methodology (Karthikeyan *et al.* 2014). Liquid phase reduction is one of the more common methods for the preparation of Cu_2O and, here, selection of the reductant is a key factor; the most commonly used reductants are glucose (Kumar *et al.* 2016), hydrazine hydrate (Wang *et al.* 2010), ascorbic acid (Bai & Dang 2015) and maltose (Wu *et al.* 2015). Since the photocatalytic activity of Cu_2O nanoparticles is closely dependent upon particle size, surfactants or templates have typically been used to suppress agglomeration of the Cu_2O nanoparticles. The most commonly used templates are cetyltrimethyl ammonium bromide (CTAB; Duan *et al.* 2012), sodium dodecyl sulfate (SDS; Yu *et al.* 2012) and anodic aluminum oxide (AAO; Musselman *et al.* 2020). Zhang *et al.* synthesized differently shaped Cu_2O nanoparticles using poly(vinyl pyrrolidone) (PVP) as the surfactant (Zhang *et al.* 2007), while Luo *et al.* synthesized hollow Cu_2O spheres, with a diameter of ~5 nm, using aerosol OT/sodium dodecyl benzene sulfonate (AOT/SDBS) vesicles with Cu^{2+}-4-ethylpyridine as the soft template (Luo *et al.* 2018). These methods have several disadvantages, including low yield, high cost and complex synthetic techniques. Template-free synthesis of Cu_2O should produce a relatively clean surface and we now report the preparation of Cu_2O nanoparticles using an

ion exchange method, without the need for surfactants. The Cu_2O nanoparticles were synthesized from cupric hydroxide ($Cu(OH)_2$) gel, which was prepared by treatment of cuprous chloride ($CuCl_2$) with anion exchange resin (AER). The main component of AERs is polystyrene, which can modify the $Cu(OH)_2$ precursor through a mechanochemical reaction and, consequently, suppress agglomeration of the $Cu(OH)_2$ particles. During the reaction, hydroxide is released slowly to produce a uniform precipitate, and the shear forces between the resins beads promote uniform dispersion of the nanoparticles. Mechanical and chemical effects can also modify particles and suppress nanoparticle agglomeration and, for comparison, $Cu(OH)_2$ precursor was also prepared by reaction of sodium hydroxide with $CuCl_2$. We term this method of preparation of Cu_2O a chemical precipitation method.

The crystal structure and morphology of the Cu_2O nanoparticles were investigated by X-ray diffraction (XRD), attenuated total reflectance Fourier transform infrared spectroscopy (ATR-FTIR) and scanning electron microscopy (SEM). The photocatalytic activity of the Cu_2O was determined by measuring the rate of degradation of methylene blue (MB) under visible light irradiation. Photocorrosion of Cu_2O was shown to be inhibited by hydrogen peroxide as a sacrificial agent, and the mechanism of this protection is discussed.

2. EXPERIMENTAL

2.1. Preparation of cuprous oxide

All chemicals used in this work were analytical grade and were used as received.

2.1.1. By ion exchange route (Sample 1)

Cupric chloride solution was added to AER (201 × 7) under continuous stirring at room temperature, producing an immediate blue gel. Once the reaction was complete, the gel was separated and added to a vigorously stirred alkaline (pH = 11) solution of glucose at 75 °C. After 1 h, the reaction mixture was filtered and the precipitate was washed several times with distilled water to pH 7. The precipitate was then dried in a furnace at 40 °C for 12 h to provide Cu_2O nanoparticles (Sample 1).

2.1.2. By chemical precipitation (Sample 2)

Aqueous sodium hydroxide solution was added to aqueous cuprous sulfate solution under constant stirring, producing an immediate flocculent blue precipitate. The reaction mixture was then stirred vigorously at 75 °C during the addition of aqueous glucose solution. After 1 h, the mixture was filtered and the precipitate was washed several times with distilled water to pH 7. The precipitate was then dried in a furnace at 40 °C for 12 h to provide Cu_2O particles (Sample 2).

2.2. Photocatalytic activity

Sample 1 was used to degrade MB under a 500 W Xe lamp, located at a distance of approximately 30 cm. Sample 1 (150 mg) was added to an aqueous solution of MB (50 mg/L, 150 mL) and the mixture was stirred magnetically for 0.5 h in the dark to reach adsorption–desorption balance. The Xe lamp was then switched on. Aliquots (5 mL) of the solution were removed every 10 min and rapidly filtered. Absorbance was measured at $\lambda = 665$ nm, using a 722 visible spectrophotometer (Peak Instruments Co., China) and the concentration of MB was calculated using the Beer-Lambert law. A standard working curve ($y = 0.1846x + 0.00739$) was obtained, with a correlation coefficient of 0.9997. The efficiency of photocatalytic degradation (η) of MB in solution was calculated using Equation (1).

$$\eta = \left\{\frac{C_0 - C_t}{C_0}\right\} \times 100\% = \left\{1 - \frac{C_t}{C_0}\right\} \times 100\% \quad (1)$$

where C_0 is the initial concentration of MB and C_t is the equilibrium concentration of MB after photocatalytic degradation.

2.3 Characterization

The surface morphology of the Cu_2O samples was investigated using a Sigma scanning electron microscope (Zeiss Co., Germany), operating at 10 kV. ATR-FTIR spectra of the samples were recorded with a Tensor 27 spectrometer (Bruker Co., Germany) over the range 4,000–400 cm^{-1}, with a resolution of 4 cm^{-1}, using KBr discs

prepared with spectral grade KBr pellets. XRD patterns were recorded using an Empyrean X-ray diffractometer (PANalytical Co., Netherlands) over the range $2\theta = 10–80°$, with Cu Kα radiation and a scan rate of 0.02 s^{-1}.

3. RESULTS AND DISCUSSION

3.1. Mechanism of preparation of copper hydroxide precursor

The decision to prepare the copper hydroxide ($Cu(OH)_2$) precursor to the Cu_2O nanoparticles using AER was based mainly on the concept of homogeneous precipitation, with the proposed mechanism illustrated in Figure 1. Firstly, Cl^- ions diffuse from the bulk solution phase into the micropores of the AER through the boundary liquid film, allowing an exchange reaction with OH^- ions. The OH^- ions then enter the bulk solution phase and reacts with Cu^{2+} ions to form $Cu(OH)_2$ (Kumar & Jain 2013). The slow release of OH^- through the ion exchange process effectively reduces the rate of formation of the $Cu(OH)_2$ gel and thus achieves homogeneous precipitation.

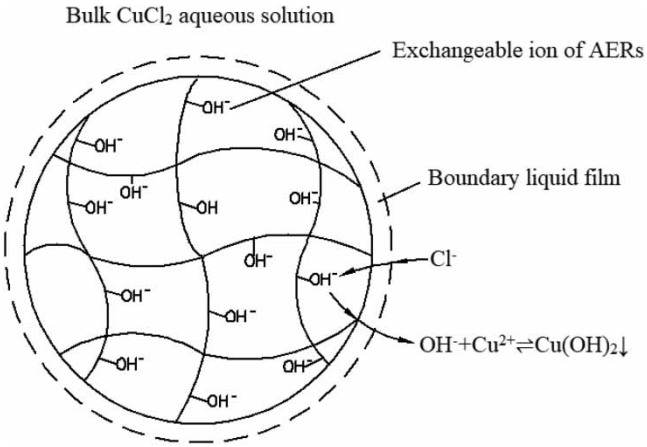

Figure 1 | Mechanism of preparation of $Cu(OH)_2$ precursor to Cu_2O nanoparticles by the ion exchange method.

Photographs of the $Cu(OH)_2$ precursors to Sample 1 and Sample 2 are shown in Figure 2. The gel prepared using the ion exchange method was uniform and light blue in color; the flocculent precipitate of $Cu(OH)_2$ prepared by chemical precipitation was a deeper blue and its distribution was not uniform.

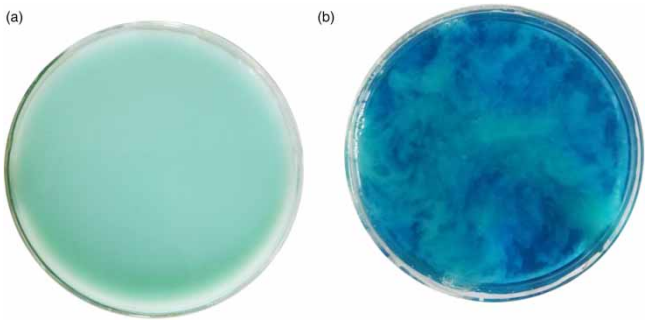

Figure 2 | Photographs of (a) $Cu(OH)_2$ precursor to Sample 1; (b) $Cu(OH)_2$ precursor to Sample 2.

3.2. SEM images

SEM images of the AER show that the surface of the resin is covered by $Cu(OH)_2$ gel, with irregular morphology (Figure 3(a, a1)). The AER must thus be washed with dilute hydrochloric acid before regeneration to remove $Cu(OH)_2$ gel from the surface.

The SEM images of Sample 1 (Figure 3(b, b1)) show that the Cu_2O is in the form of uniform spheres, with smooth surfaces and no obvious aggregation. The SEM images of Sample 2 (Figure 3(c, c1)), by contrast, show that the particle size distribution is not uniform, due to aggregation of the Cu_2O particles.

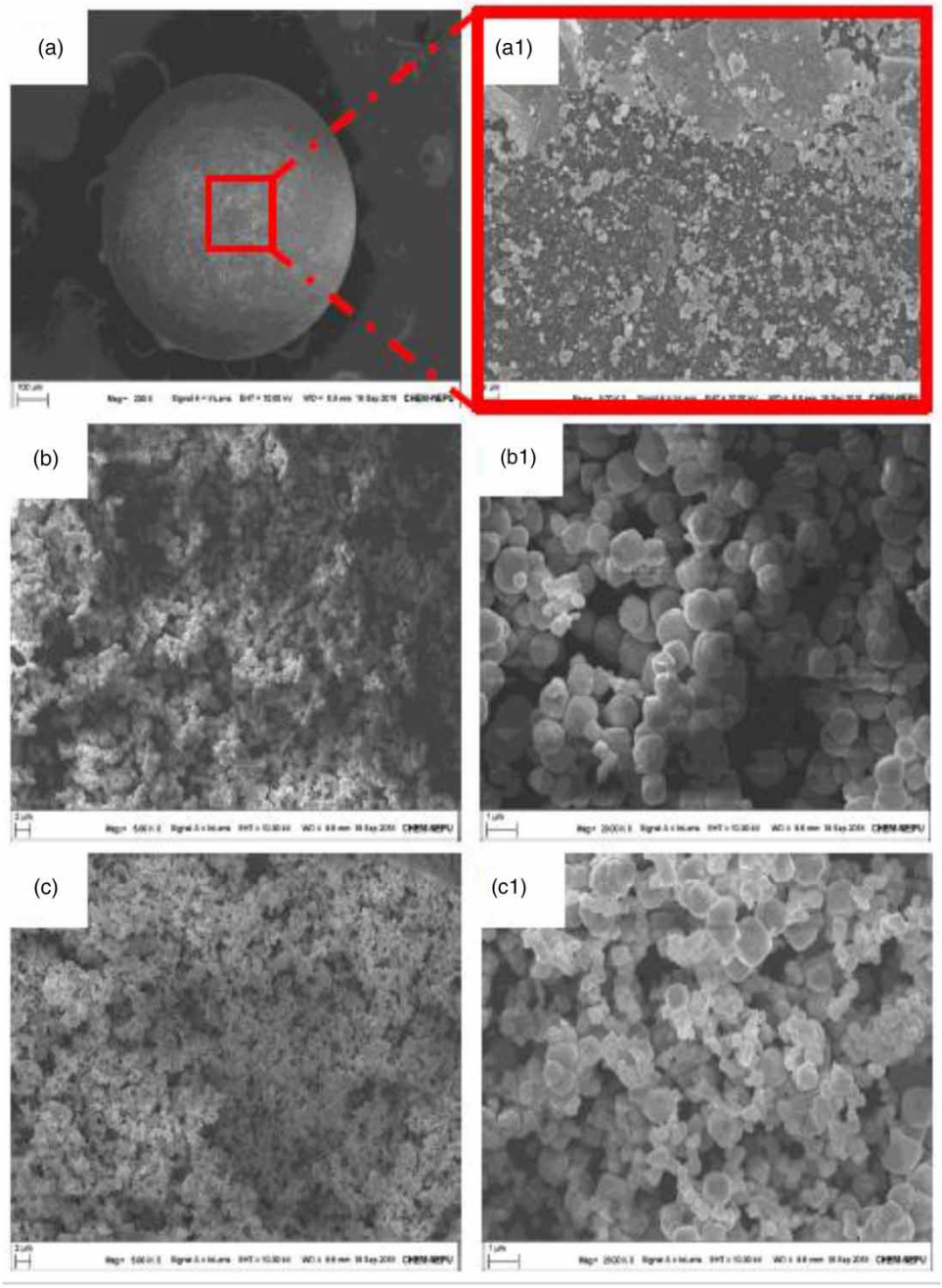

Figure 3 | SEM images of (a, a1) AER after reaction; (b, b1) Sample 1; (c, c1) Sample 2.

The SEM images show that the Cu_2O nanoparticles in Sample 1 have a more uniform size (400–1,200 nm) than those in Sample 2 (200–2,400 nm) (Figure 4(a) and 4(b)). The average diameters of the nanoparticles in Sample 1 and Sample 2 are 780 and 1,100 nm, respectively. These results confirm that the ion exchange method plays a key role in reducing or eliminating aggregation of the Cu_2O nanoparticles.

Different methods of preparation of Cu_2O nanomaterials are shown in Table 1. Compared with other synthetic strategies, the work described in this paper is low cost and easy to operate. The Cu_2O nanoparticles prepared by our method do, however, have both larger size and wider particle size distribution than most of those produced using other methods, which means that our method requires further refinement.

3.3. ATR-FTIR analysis

The ATR-FTIR spectra of Sample 1 and Sample 2 are shown in Figure 5. The broad absorption peaks around 627 cm^{-1} correspond to the characteristic peak of Cu_2O (Shangguan *et al.* 2016). There were no other

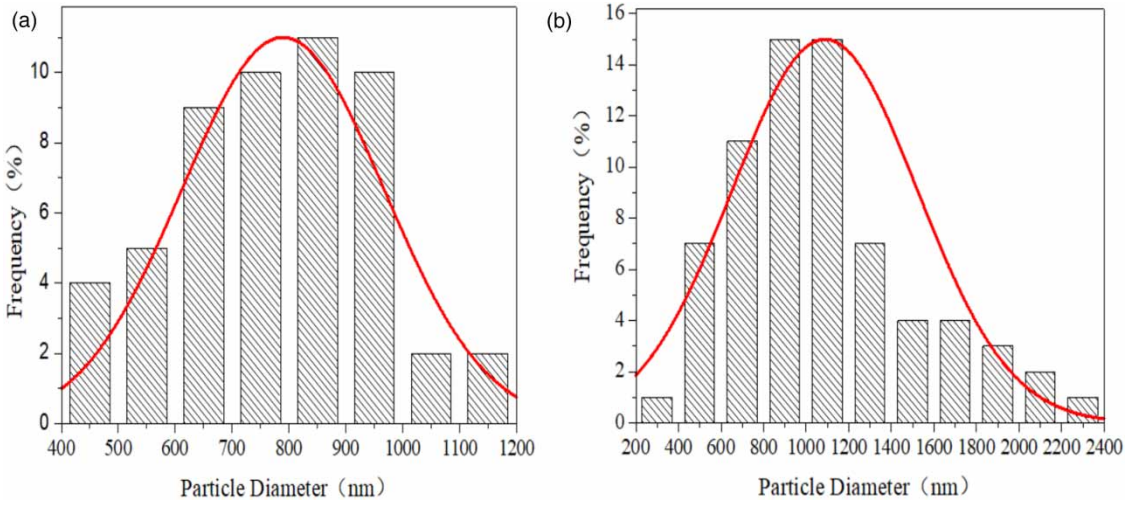

Figure 4 | Particle size distributions of (a) Sample 1; (b) Sample 2.

significant absorption peaks in the spectrum of Sample 2. The additional peaks in the spectrum of Sample 1 at 1,463 and 3,140 cm^{-1} were attributed to C–H bending vibrations, the additional peaks at 2,853 cm^{-1} were assigned to antisymmetric stretching vibrations of methylene (CH_2) groups and the absorption peak at 1,550 cm^{-1} was attributed to the benzene ring skeleton (Shangguan *et al.* 2016). These results demonstrate that the Cu_2O nanoparticles have been modified by polystyrene, which is the main component of the AER, and explain how the ion exchange method effectively limits aggregation of the Cu_2O nanoparticles.

3.4. XRD analysis

The XRD patterns of both Sample 1 and Sample 2 (Figure 6) show diffraction peaks at $2\theta = 29°$, 36°, 42°, 62°, 73° and 77°, corresponding to the {110}, {111}, {200}, {220}, {311} and {222} crystal planes, respectively, of Cu_2O (JCPDS No.78-2076) (Zhang *et al.* 2010). The diffraction patterns show no signs of impurities, such as Cu, CuO or $Cu(OH)_2$, indicating that both samples consist of pure Cu_2O. The similarity of the XRD patterns of the two samples shows that the precursor has little influence on the crystal structure of the Cu_2O nanoparticles.

3.5. Photocatalytic activity

During the photocatalytic degradation of MB by Cu_2O, strongly oxidizing hydroxyl radicals (·OH) are formed on the surface of the Cu_2O nanoparticles. During the reaction, not only is MB degraded by the ·OH radicals, but the Cu_2O itself is also partially oxidized, eventually resulting in nanoparticles with reduced photocatalytic activity and poor stability, a phenomenon known as photocorrosion (Cui *et al.* 2022).

We encountered this problem in our study. In the absence of hydrogen peroxide (H_2O_2), the removal ratio of MB first increases and then decreases, 44.7% of the MB was degraded during the first 10 min of the photocatalytic reaction, whereas only 19.2% was degraded during the 60 min experiment (Figure 7(a)).

The addition of H_2O_2 to the reaction system inhibits photocorrosion of the Cu_2O nanoparticles. When the reaction system contained 10 wt% H_2O_2, the removal ratio of MB increased continuously as the reaction time was increased (Figure 7(b)). During the first 10 min of the reaction, 52.7% of the MB was degraded, which is somewhat more than is degraded during the first 10 min in the absence of H_2O_2. After 90 min, 97.2% of the MB had been degraded, showing that the photocatalytic activity of Cu_2O is improved in the presence of H_2O_2. When the reaction system contained 7.5 wt% H_2O_2, 80.7% of the MB was degraded

Table 1 | Comparation of synthetic strategies for synthesis of Cu_2O nanomaterials

Cu^{2+} source	Reductant	Template	Preparation conditions	Product name and structure	Ref.
$CuCl_2{\cdot}2H_2O$	Glucose	PEG	Reaction time, 30 min; reaction temperature, 50 °C; dried in vacuum oven at 40 °C for 12 h.	Cu_2O; cubic architecture; particle size, 375 nm.	Kumar *et al.* (2016)
$CuSO_4{\cdot}5H_2O$	Hydrazine hydrate	Not used	Reaction time, 15 min; reaction temperature: room temperature; dried at 30 °C.	Cu_2O; hollow microspheres; particle size, 0.7–7 μm.	Wang *et al.* (2010)
$CuCl_2{\cdot}2H_2O$	Ascorbic acid	Not used	Reaction temperature, room temperature.	Cu_2O; litchi-shaped; particle size, 100 nm.	Bai & Dang (2015)
$CuSO_4{\cdot}5H_2O$	Maltose	Not used	Reaction time, 2 h; reaction temperature, 80 °C.	Cu_2O nanoparticles supported on reduced graphene oxide; hollow spherical structure; particle size, 200 nm.	Wu *et al.* (2015)
$CuSO_4{\cdot}5H_2O$	Na_2SO_3	CTAB	Reaction time, 2 h; reaction temperature, 90 °C; pH 6; dried in vacuum oven at 70 °C for 10 h.	One-dimensional Cu_2O crystals; particle size, 5–10 μm.	Duan *et al.* (2012)
$CuSO_4$	hydrazine hydrate	SDS	Reaction time, 40 min; reaction temperature, 20 °C; dried in vacuum oven at 50 °C for 6 h.	Cu_2O; hollow porous microspheres; particle size, 200–500 nm.	Yu *et al.* (2012)
$CuSO_4$	Non	AAO	Electrodeposition method; graphite electrode used as a counter electrode and saturated calomel electrode used as a reference electrode.	Cu_2O nanowires.	Musselman *et al.* (2020)
$Cu(NO_3)_2{\cdot}3H_2O$	Ethylene glycol	PVP	Reaction time, 2 h; reaction temperature, 160 °C.	Cu_2O; average diameter and length of nanorods, 70 and 700 nm; spherical; average size, ~260 nm.	Zhang *et al.* (2007)
$Cu(OAc)_2$	Ascorbic acid	AOT/SDBS vesicles with Cu^{2+}-4-ethylpyridine	Reaction time, 1.5 h; reaction temperature, 25 °C; dried in vacuum drying oven at 40 °C for 6 h.	Cu_2O; hollow spheres; particle size, ~5 nm.	Luo *et al.* (2018)
$Cu(OH)_2$ gel prepared by the ion exchange method	Glucose	Not used	Reaction time, 1 h; reaction temperature, 75 °C, pH 11; dried in furnace at 40 °C for 12 h.	Cu_2O; microspheres; particle size, 780 nm.	This work

in the first 10 min. If the concentration of H_2O_2 was further reduced to 4.5% or 1.5%, less MB was degraded in the first 10 min of the reaction, possibly because of reduction of amounts of hydroxyl radicals. Only 9.26% of the MB was degraded after 90 min in a reaction system containing 7.5 wt% H_2O_2 but no

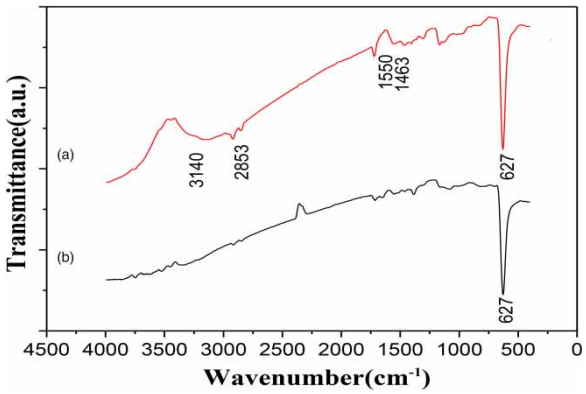

Figure 5 | ATR-FTIR spectra of (a) Sample 1; (b) Sample 2.

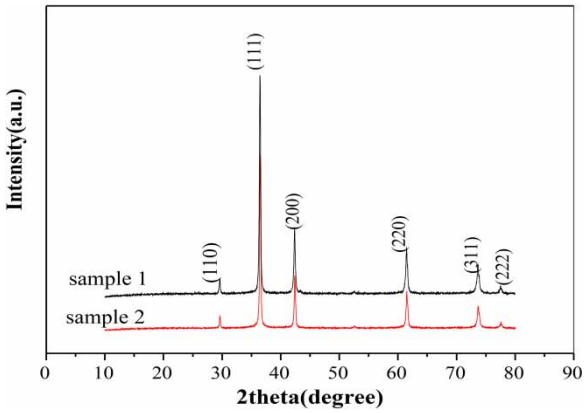

Figure 6 | XRD patterns of Sample 1 and Sample 2.

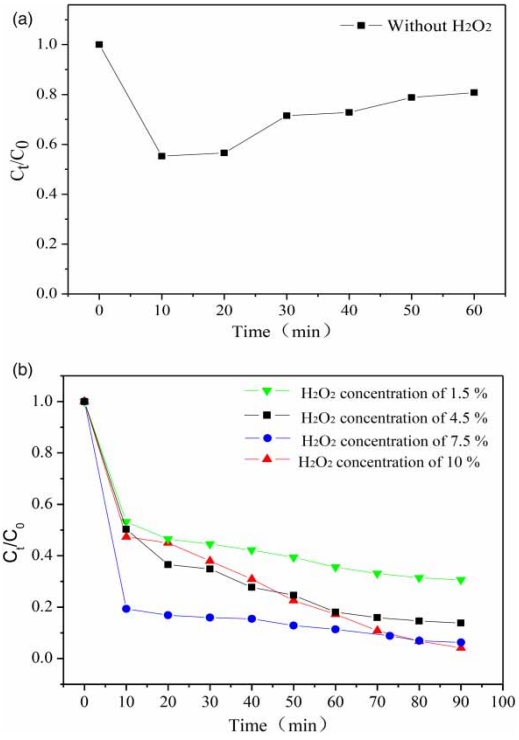

Figure 7 | Effect of hydrogen peroxide on photocatalysis degradation of MB.

Cu_2O, confirming that the photocatalyst Cu_2O plays a crucial role in this reaction.

$$Cu_2O + hv \rightarrow h^+ + e^- \quad (2)$$

$$e^- + O_2 \rightarrow {}^{\cdot}O_2^- \quad (3)$$

$${}^{\cdot}O_2^- + H_2O_2 \rightarrow {}^{\cdot}OH + OH^- \quad (4)$$

$${}^{\cdot}OH + MB \rightarrow \text{intermediates} \rightarrow \text{degraded products} \quad (5)$$

H_2O_2 inhibits photocorrosion mainly because superoxide radicals ($\cdot O_2^-$) generated in the presence of Cu_2O under visible light irradiation (Equations (2) and (3) react with H_2O_2 and produce ·OH radicals (Cheng *et al.* 2022; Meng *et al.* 2022; Equation (4)). These ·OH radicals can then oxidize and degrade MB, increasing photocatalytic degradation (Equation (5)). The H_2O_2 also acts as a sacrificial agent by directly reducing interactions between the Cu_2O and the strongly oxidizing, newly generated superoxide radicals.

4. CONCLUSION

In summary, Cu_2O nanoparticles, with an average particle size <800 nm were successfully prepared by an ion exchange method, using $Cu(OH)_2$ gel as a precursor. The polystyrene in the ion exchange resin modifies the Cu_2O nanoparticles and reduces or eliminates agglomeration. The Cu_2O nanoparticles are effective catalysts for the photodegradation of MB, and hydrogen peroxide effectively inhibits photocorrosion of the Cu_2O nanoparticles during the photocatalytic reaction.

ACKNOWLEDGEMENTS

This work was supported by the Foundation of Key Laboratory of Pulp and Paper Science and Technology of the Ministry of Education, Shandong Province of China (KF201826), the NEPU Scientific Research Foundation (rc201726) and the National Natural Science Foundation of China (201606042).

DATA AVAILABILITY STATEMENT

All relevant data are included in the paper or its Supplementary Information.

CONFLICT OF INTEREST

The authors declare there is no conflict.

REFERENCES

Bai, L. & Dang, Z. 2015 Facile synthesis of litchi shaped cuprous oxide and its application in the aerobic oxidative synthesis of imines. *RSC Advances* **5**(14), 10341–10345.

Cheng, Y., Cao, T., Xiao, Z., Zhu, H. & Yu, M. 2022 Photocatalytic treatment of methyl orange dye wastewater by porous floating ceramsite loaded with cuprous oxide. *Coatings* **12**(2), 286.

Cui, L. K., Hu, L. Q., Shen, Q. Q., Liu, X. G., Jia, H. S. & Xue, J. B. 2022 Three-dimensional porous Cu_2O with dendrite for efficient photocatalytic reduction of CO_2 under visible light. *Applied Surface Science* **581**, 152343.

Duan, X., Zhang, Y., Gao, R., Jian, Z., Zhao, Y., Liu, W. & Gao, Y. 2012 Synthesis of 1-D cuprous oxide by using CTAB as a soft template in an acidic system. *Materials Letters* **68**, 146–148.

Karthikeyan, B., Udayabhaskar, R., Rose, T. P., Pandiyarajan, T. & Philip, R. 2014 Sol-gel prepared Cu_2O microspheres: linear and nonlinear optical properties. *RSC Advances* **4**(74), 39541–39546.

Kumar, S. & Jain, S. 2013 History, introduction, and kinetics of ion exchange materials. *Journal of Chemistry* **2013**, 1–13.

Kumar, S., Parlett, C. M. A., Isaacs, M. A., Jowett, D. V., Douthwaite, R. E., Cockett, M. C. R. & Lee, A. F. 2016 Facile synthesis of hierarchical Cu_2O nanocubes as visible light photocatalysts. *Applied Catalysis B: Environmental* **189**, 226–232.

Kuo, C. Y., Wu, C. H., Wu, J. T. & Chen, Y. C. 2014 Preparation of immobilized Cu_2O using microwave irradiation and its catalytic activity for bisphenol A: comparisons of Cu_2O/H_2O_2 and visible-light/Cu_2O/H_2O_2 systems. *Water Science and Technology* **70**(8), 1428–1433.

Luo, X. L., Pan, Z., Pei, F., Jin, Z. P., Miao, K. K., Yang, P. F., Qian, H. M., Chen, Q. & Feng, G. D. 2018 In situ growth of hollow Cu_2O spheres using anionic vesicles as soft templates. *Journal of Industrial and Engineering Chemistry* **59**, 410–415.

Meng, X., Zhou, K., Qian, Y., Liu, H., Wang, X., Lin, Y., Shi, X., Tian, Y., Lu, Y., Chen, Q., Qian, J. & Wang, H. 2022 Hollow cuprous oxide@nitrogen-doped carbon nanocapsules for cascade chemodynamic therapy. *Small* **18**(15), 2107422.

Musselman, K. P., Delumeau, L.-V., Araujo, R., Wang, H. & MacManus-Driscoll, J. 2020 Electrochemical removal of anodic aluminium oxide templates for the production of phase-pure cuprous oxide nanorods for antimicrobial surfaces. *Electrochemistry Communications* **120**, 106833.

Muthukumaran, M., Gnanamoorthy, G., Prasath, P. V., Abinaya, M., Dhinagaran, G., Sagadevan, S., Mohammad, F., Oh, W. C. & Venkatachalam, K. 2020 Enhanced photocatalytic activity of cuprous oxide nanoparticles for malachite green degradation under the visible light radiation. *Materials Research Express* **7**(1), 051038.

Shangguan, W. W., Gong, Y. C., Zhao, R. J. & Ren, H. Q. 2016 Effects of heat treatment on the properties of bamboo scrimber. *Journal of Wood Science* **62**(5), 383–391.

Sun, Y. C., Sun, C. Y., Chen, Z. X., Wang, P., Wang, H. T., Yao, M. Z., Wu, S. & Xu, P. 2021 Morphology control of Cu and Cu_2O through electrodeposition on conducting polymer electrodes. *Inorganic Chemistry Frontiers* **8**(6), 1449–1454.

Wang, N., He, H. C. & Han, L. 2010 Room temperature preparation of cuprous oxide hollow microspheres by a facile wet-chemical approach. *Applied Surface Science* **256**(23), 7335–7338.

Wu, C. K., An, X. Y., Gao, S. Y. & Su, L. 2015 Self-assembly of cuprous oxide nanoparticles supported on reduced graphene oxide and their enhanced performance for catalytic reduction of nitrophenols. *RSC Advances* **5**(87), 71259–71267.

Yu, Y., Zhang, L., Wang, J., Yang, Z., Long, M., Hu, N. & Zhang, Y. 2012 Preparation of hollow porous Cu_2O microspheres and photocatalytic activity under visible light irradiation. *Nanoscale Research Letters* **7**, 347.

Yu, X. J., Kou, S., Zhang, J., Tang, X. Y., Yang, Q. & Yao, B. H. 2018 Preparation and characterization of Cu_2O nano-particles and their photocatalytic degradation of fluroxypyr. *Environmental Technology* **39**(22), 2967–2976.

Zhang, H., Ren, X. & Cui, Z. L. 2007 Shape-controlled synthesis of Cu_2O nanocrystals assisted by PVP and application as catalyst for synthesis of carbon nanofibers. *Journal of Crystal Growth* **304**(1), 206–210.

Zhang, X., Song, J., Jiao, J. & Mei, X. 2010 Preparation and photocatalytic activity of cuprous oxides. *Solid State Sciences* **12**(7), 1215–1219.

First received 26 April 2022; accepted in revised form 6 January 2023. Available online 18 January 2023